Ray Tracing Near the Electron Cyclotron Frequency with Application to EBT

D. B. BATCHELOR, R. C. GOLDFINGER, AND H. WEITZNER

Abstract—The general problem of ray tracing in the electron cyclotron range of frequencies is addressed with the view of applying geometrical optics techniques to microwave heating in ELMO Bumpy Torus (EBT). It is shown that the usual formulation of geometrical optics breaks down at cyclotron resonance due to the large anti-Hermitian part of the dispersion tensor. A consistent eikonal expansion is presented which is valid near cyclotron resonance for cases in which the waves are weakly damped. The geometrical optics code, RAYS, which was developed for the EBT study is described. Ray tracing in plane-stratified plasma geometries is discussed and examples given of the various types of ray paths which occur in plasmas stratified perpendicular to the magnetic field and stratified along magnetic field lines. The application of ray tracing techniques to EBT is discussed and typical results are presented of rays traced in a bumpy cylinder magnetic-field configuration with plasma parameters characteristic of EBT-I.

I. Introduction

THE METHODS OF geometrical optics are finding application in the study of wave heating processes and instabilities for a wide range of fusion research devices. Studies of plasma heating near the electron cyclotron frequency are particularly amenable to ray tracing techniques because of the high frequencies and short free-space wavelengths involved ($\lambda \leqslant 2$ cm) [1], [2]. Successful electron cyclotron heating (ECH) experiments have been conducted in a number of tokamaks, multipoles, and mirror machines. However, in no devices is ECH more necessary to the operation and ray tracing techniques more necessary to understanding the physics than in ELMO Bumpy Torus (EBT) [3]. In EBT the plasma is produced and all heating is provided by microwaves through the electron cyclotron resonance interaction. In addition, the microwaves play an essential role by producing the high-beta hot electron annuli which provide macroscopic stability for the toroidal plasma component. Therefore, a knowledge of the microwave field distribution and heating profile is crucial to the understanding of EBT physics. However, the geometry and plasma conditions in EBT are such that solving for the microwave fields by full-wave methods is totally impractical. As a result, we have begun a large-scale computational effort to study the microwave energy flow and energy deposition using geometrical optics.

Manuscript received September 22, 1979; revised November 7, 1979. This research was sponsored by the Office of Fusion Energy, U.S. Department of Energy, under Contract W-7405-ENG-26 with the Union Carbide Corporation.

D. B. Batchelor is with the Fusion Energy Division, Oak Ridge National Laboratory, Oak Ridge, TN 37830.

R. C. Goldfinger is with the Computer Sciences Division, Oak Ridge National Laboratory, Oak Ridge, TN 37830.

H. Weitzner is with the Courant Institute of Mathematical Sciences, New York University, New York, NY 10012.

The purpose of this paper is to review the properties of electromagnetic wave propagation near the electron cyclotron frequency, to describe the geometrical optics computer code (RAYS) which we have developed, and to discuss the application of ray tracing methods to ECH problems in EBT. In Section II we discuss some of the difficulties which arise in applying the geometrical optics formalism at the electron cyclotron frequency. Because the anti-Hermitian part of the dispersion tensor becomes large at cyclotron resonance, the usual formulation of geometrical optics breaks down. However, by simultaneously expanding Maxwell's equations and the Vlasov equation in the geometrical optics parameter, we obtain a rigorous theory which is valid near cyclotron resonance in cases where the waves are weakly damped. In Section III we give a brief description of the ray tracing code.

In a plane-stratified plasma, ray tracing is considerably simplified in that only the component of the wave vector $\tilde{k}$ which is in the direction of the gradients can vary. The location of cutoffs, resonances, and mode conversion points, and the behavior of $\tilde{k}$ and the ray trajectory can, therefore, be determined directly from the dispersion relation without actually tracing rays. Ray tracing in plane-stratified geometry serves as a valuable check on the accuracy of the code and also allows many interesting properties of wave propagation in inhomogeneous plasmas to be illustrated in the simplest possible geometry. In Section IV we discuss in detail wave propagation near the cyclotron frequency in plane-stratified plasmas and present computed ray trajectories. We also present results of ray tracing with a finite temperature-dispersion relation showing conversion of extraordinary mode rays to electrostatic warm plasma modes.

In Section V we describe the EBT device and discuss the ray tracing approach being used to calculate the microwave propagation and energy deposition characteristics. Typical results are presented of ray calculations in a bumpy cylinder plasma configuration having parameters appropriate for EBT-I. Results such as these in the complicated geometry of EBT cannot be obtained without the use of ray tracing techniques.

II. The Ray Tracing Equations

The theory of geometrical optics [4]-[6] seeks to describe the propagation of waves in an inhomogeneous medium by expanding the wave equations in a parameter $\delta = \lambda/L$, assumed small. Here λ is the wavelength and L is a characteristic scale length of variation of the medium. To zero order in δ, one obtains equations for the direction of energy flow (ray paths) and for changes in the wave vector $\tilde{k}$ as one moves along the ray path. In order to obtain information concerning the am-

plitude of the fields, it is necessary to go to first order in the formal δ expansion. See reference [5] for a derivation relevant to plasmas.

For application to problems of plasma heating, propagation of waves to and through cyclotron resonances is a matter of no small importance. Despite the fact that waves can be weakly damped and $\tilde{k}$ can be slowly varying near a cyclotron resonance (e.g., ordinary mode or extraordinary mode propagating nearly perpendicular to the magnetic field), the standard formulations of geometrical optics break down near cyclotron resonances. Since the physical conditions for the validity of the geometrical optics actually are met in many cases, it should be possible to formulate a geometrical optics-like approximation which is valid uniformly near and far from cyclotron harmonic resonances. We have, in fact, recently obtained an eikonal expansion which is valid in finite temperature plasmas near cyclotron resonance [7]. The ray trajectories are found to coincide with those given by cold plasma theory, but Poynting's theorem is somewhat modified from the standard result.

In order to see how the standard theory breaks down, we outline the derivation of the ray equations and Poynting's theorem (see reference [5]). We assume a weakly space- and the time-varying plasma and assume the wave fields to have a rapidly varying phase $\psi(\tilde{x}, t)$ and a slowly varying amplitude

$$\tilde{\mathcal{E}}(\tilde{x}, t) = \mathrm{Re}\ \{\tilde{E}(\tilde{x}, t)\, e^{i\psi(\tilde{x}, t)}\} \tag{1}$$

where

$$\left|\frac{\partial \tilde{E}}{\partial t}\right| \ll |\omega \tilde{E}|, \left|\frac{\partial \tilde{E}}{\partial \tilde{x}}\right| \ll |\tilde{k}\tilde{E}|, \qquad \text{and}$$

$$\omega \equiv -\frac{\partial \psi}{\partial t}, \tilde{k} \equiv \frac{\partial \psi}{\partial x}.$$

The plasma is described by a nonlocal causal constitutive relation

$$\begin{aligned}\tilde{J}(\tilde{x}, t) &= \int d^3x' \int_{-\infty}^{t} dt' \tilde{\tilde{\sigma}}(\tilde{x} - x', t - t') \cdot \tilde{\mathcal{E}}(\tilde{x}', t') \\ &= \int d^3x' \int_{0}^{\infty} dt' \tilde{\tilde{\sigma}}(\tilde{x}', t') \\ &\quad \cdot \tilde{\mathcal{E}}(\tilde{x} - \tilde{x}', t - t')\, e^{i\psi(\tilde{x} - \tilde{x}', t - t')}.\end{aligned} \tag{2}$$

If $\tilde{\tilde{\sigma}}(x, t)$ is sufficiently peaked near $x = 0$, $t = 0$, then we can expand $\tilde{\mathcal{E}}(x - x', t - t')$ about x', t'. Then

$$\tilde{\mathcal{E}}(\tilde{x} - \tilde{x}', t - t') \cong \left(1 - \tilde{x}' \cdot \tilde{\nabla} - t' \frac{\partial}{\partial t} + \cdots\right) \tilde{\mathcal{E}}(\tilde{x}, t). \tag{3}$$

Introducing the Fourier transform of $\tilde{\tilde{\sigma}}(\tilde{x}, t)$

$$\tilde{\tilde{\sigma}}(\tilde{k}, \omega) = \int d^3x \int_{0}^{\infty} dt\, \tilde{\tilde{\sigma}}(\tilde{x}, t)\, e^{-i(\tilde{k} \cdot \tilde{x} - \omega t)}. \tag{4}$$

The current density can be expressed

$$\tilde{J}(\tilde{x}, t) \cong \left[\tilde{\tilde{\sigma}}(\tilde{k}, \omega) \cdot \tilde{E} - i \frac{\partial \sigma_{ij}}{\partial k_l} \frac{\partial E_j}{\partial x_l} + i \frac{\partial \tilde{\tilde{\sigma}}}{\partial \omega} \cdot \frac{\partial \tilde{E}}{\partial t}\right] e^{i\psi(\tilde{x}, t)}. \tag{5}$$

We now do a formal expansion of Maxwell's equations in the small parameter δ where it is assumed that $|\partial \tilde{E}/\partial \tilde{x}|/k \sim |\partial \tilde{E}/\partial t|/\omega \sim \delta$. We also make the assumption (and this is crucial) that $\tilde{\tilde{\sigma}}^H \sim \delta \tilde{\tilde{\sigma}}^A$, where $\tilde{\tilde{\sigma}}^H$ and $\tilde{\tilde{\sigma}}^A$ are the Hermitian and anti-Hermitian parts of, respectively, $\tilde{\tilde{\sigma}}^H = \frac{1}{2}(\tilde{\tilde{\sigma}} + \tilde{\tilde{\sigma}}^+)$, $\tilde{\tilde{\sigma}}^A = \frac{1}{2}(\tilde{\tilde{\sigma}} - \sigma^+)$. In general, the presence of $\tilde{\tilde{\sigma}}^H$ results in absorption of the waves, so the ordering $|\tilde{\tilde{\sigma}}^H| \ll \delta |\tilde{\tilde{\sigma}}^A|$ ensures that the waves are weakly damped, a requirement for geometrical optics to make sense. However, as we shall see, it is not at all necessary that $\tilde{\tilde{\sigma}}^H$ be small in order to have weakly damped waves.

Using (3) and (5) in Maxwell's equations gives in zero order

$$\tilde{\tilde{D}}^H \cdot \tilde{E} = 0 \tag{6}$$

where

$$\tilde{\tilde{D}}^H = \left(1 - \frac{c^2 k^2}{\omega^2}\right) \tilde{\tilde{I}} + \frac{c^2}{\omega^2} \tilde{k}\tilde{k} + \frac{4\pi i}{\omega} \tilde{\tilde{\sigma}}^A$$

with the solvability condition (dispersion relation)

$$D(\tilde{k}, \omega, \omega_{pe}, \Omega_e, t) = \det\, [\tilde{\tilde{D}}^H] = 0. \tag{7}$$

Equation (7) can be regarded as a partial differential equation for $\psi(\tilde{x}, t)$, $D[(\partial\psi/\partial \tilde{x}), -(\partial\psi/\partial t), \omega_{pe}(\tilde{x}), \Omega_e(\tilde{x})] = 0$. Solving (7) for $\omega = \omega(\tilde{k}, \tilde{x}, t)$ and using the conservation law $\tilde{\nabla}\omega + \partial \tilde{k}/\partial t = 0$ gives the ray equations

$$\frac{\partial \tilde{x}}{\partial t} \equiv \tilde{v}_g = \frac{\partial \omega}{\partial \tilde{k}} = -\frac{\partial D/\partial \tilde{k}}{\partial D/\partial \omega} \qquad \frac{\partial \tilde{k}}{\partial t} = -\frac{\partial \omega}{\partial \tilde{k}} \equiv \frac{\partial D/\partial \tilde{x}}{\partial D/\partial \omega}. \tag{8}$$

Note that by taking $\tilde{\tilde{\sigma}}^H$ to be first order in δ we have guaranteed that $\tilde{\tilde{D}}^H$ is Hermitian, which implies that the dispersion relation equation (7) is real. As a result, the ray trajectories determined by (8) stay in real space.

The first-order Maxwell's equations can be used to obtain the standard Poynting's theorem of the form

$$\frac{\partial u}{\partial t} + \tilde{\nabla} \cdot \tilde{S} + \tilde{E}^* \cdot \tilde{\tilde{\sigma}}^H \cdot \tilde{E} = 0 \tag{9}$$

where

$$\begin{aligned} u &= \frac{1}{8\pi} \tilde{E}^* \cdot \frac{\partial}{\partial \omega} (\omega \tilde{\tilde{D}}^H) \cdot \tilde{E} \\ &= \frac{1}{8\pi} \left[|E|^2 + |B|^2 + \tilde{E}^* \cdot \frac{\partial}{\partial \omega} (4\pi i \tilde{\tilde{\sigma}}^A) \cdot E\right] \\ &= \text{wave energy density} \end{aligned}$$

$$\tilde{S} = \mathrm{Re}\left\{\frac{c}{4\pi} \tilde{E} \cdot \tilde{B} - \frac{1}{4\pi} \frac{\partial}{\partial \tilde{k}} (4\pi i \tilde{\tilde{\sigma}}^A) : \tilde{E}^* \tilde{E}\right\} = \tilde{v}_g u$$

= wave power flux.

Now let us examine what happens near cyclotron resonance. First consider a cold plasma model with $\omega \sim \Omega_e >> \Omega_i, \omega_{pi}$. The dispersion tensor is Hermitian and has typical elements of the form

$$D_{xx} = 1 - \frac{c^2 k_z^2}{\omega^2} - \frac{\omega_{pe}^2}{\omega^2 - \Omega_e^2}. \tag{10}$$

This tensor is singular at $\omega = \Omega_e$, indicating an infinitely dispersive medium. This behavior is connected with the presence

of infinitely long correlations in a lossless medium. In the space-time domain the conductivity tensor has elements of the form

$$\sigma_{xx}(\tilde{x}, t) = \frac{1}{4\pi}\frac{\omega_{pe}^2}{\omega}\cos\left[\Omega_e(t - t')\right]\delta(\tilde{x} - \tilde{x}') \tag{11}$$

which is not sharply peaked at $t = 0$, and the expansion equation (3), therefore, fails. This does not cause difficulty in practice, however, because the dispersion relation $D \equiv \det[\tilde{\tilde{D}}]$ is not singular at $\omega = \Omega_e$ and there is no resonance in $\tilde{k}$ unless $\tilde{k}$ is parallel to $\tilde{B}$. Solving for the polarization vectors $\tilde{E}$ (6), we find that $E_x \to iE_y$ as $\omega \to \Omega_e$ for both ordinary mode and extraordinary mode roots of the dispersion relation. That is, the wave becomes left circularly polarized so that the long-term correlations associated with the electron cyclotron motion are not excited. In the cold plasma model we can trace rays without difficulty near and through the cyclotron resonance unless $\tilde{k}$ is exactly parallel to $\tilde{B}$. Here the formulation is not valid but the method apparently works.

Now consider a finite temperature Maxwellian plasma. The full dispersion tensor $\tilde{\tilde{D}} = \tilde{\tilde{D}}^H + \tilde{\tilde{D}}^A$ has typical elements of the form

$$D_{xx} = 1 - \frac{c^2k^2}{\omega^2} - \frac{\omega_{pe}^2}{2\omega(\omega + \Omega_e)} + \frac{\omega_{pe}^2}{\omega k_z v_e}Z(\xi) \tag{12}$$

where $Z(\xi)$ = plasma dispersion function and $\xi = (\omega - \Omega_e)/k_z v_e$. For most plasmas of interest c/v_e is quite large, so that exactly at resonance $\tilde{\tilde{D}}^H(\omega = \Omega_e) \ll \tilde{\tilde{D}}^A(\omega = \Omega_e)$. The full dispersion relation $D = \det[\tilde{\tilde{D}}]$ obtained from (12) is complex, and its direct use in (11) would result in rays going off into complex configuration space. On the other hand, neglecting the anti-Hermitian part of D and using the real dispersion relation obtained gives results which are simply *wrong*. In this case the formulation is not valid and the method clearly does not work.

Even though $|\tilde{\tilde{D}}^A| > |\tilde{\tilde{D}}^H|$, there are large regions in parameter space where the waves are weakly damped (e.g., ordinary mode $\theta \sim 0$ and extraordinary mode $\theta \to \pi/2$). In these cases, the complex solutions $k = k_r + ik_i$ obtained from the full dispersion relation have $|k_i| \ll |k_r|$, and $\tilde{k}_r$ is very nearly equal to $\tilde{k}$ as obtained from cold plasma theory. Physically we can understand this as follows: If we solve for the polarization vectors $\tilde{E}$, we again find $E_x \cong iE_y$. The wave is nearly left circularly polarized, so the interaction with electron cyclotron motion is weak even though many particles can resonate with the wave ($\omega - \Omega_e - k_z v_z = 0$ for $v_z \cong 0$). In view of these facts, we do expect to be able to formulate a geometrical optics-like expansion with real characteristics and a real eikonal function which is valid near $\omega = \Omega_e$ for weakly damped waves.

In our procedure the linearized Vlasov equation is expanded simultaneously with Maxwell's equations. Specializing to the case of electron cyclotron waves, we assume that the wave frequency ω, the electron plasma frequency ω_{pe}, and electron cyclotron frequency are all large and comparable. We consider ω to be near cyclotron resonance $(\omega - |\Omega_e|)/\omega \sim 0(\delta)$ and assume the electron thermal speed to be much smaller than the wave phase velocity $v_e k/\omega \sim 0(\delta)$. An ansatz of the form equation (1) is assumed, and a formal small parameter δ is in-

In zeroth order the equations are just those for waves in an infinite uniform plasma

$$\left(1 - \frac{n_x^2}{2} - n_\parallel^2 + \frac{4\pi i}{\omega}\sigma_{++}\right)E_+^0 + \left(\frac{n_x^2}{2} + \frac{4\pi i}{\omega}\sigma_{+-}\right)E_-^0 + \left(n_\parallel n_x + \frac{4\pi i}{\omega}\sigma_{+\parallel}\right)E_\parallel^0 = 0 \tag{13a}$$

$$\left(\frac{n_x^2}{2} + \frac{4\pi i}{\omega}\sigma_{-+}\right)E_+^0 + \left(1 - \frac{n_x^2}{2} - n_\parallel^2 + \frac{4\pi i}{\omega}\sigma_{--}\right)E_-^0 + \left(n_\parallel n_x + \frac{4\pi i}{\omega}\sigma_{-\parallel}\right)E_\parallel^0 = 0 \tag{13b}$$

$$\left(\frac{n_\parallel n_x}{2} + \frac{4\pi i}{\omega}\sigma_{\parallel+}\right)E_+^0 + \left(\frac{n_\parallel n_x}{2} + \frac{4\pi i}{\omega}\sigma_{\parallel-}\right)E_-^0 + \left(1 - n_x^2 + \frac{4\pi i}{\omega}\sigma_{\parallel\parallel}\right)E_\parallel^0 = 0 \tag{13c}$$

where we have chosen a coordinate system with z parallel to the magnetic field, x is in the $\tilde{k}, \tilde{B}$ plane, and we have adopted the representation $E_\pm = E_x \pm iE_y$, $E_\parallel = E_z$. The conductivity tensor $\tilde{\tilde{\sigma}}$ is the standard result for a finite temperature plasma [6], [8] and is discussed in detail with this representation in reference [7]. With the ordering we have chosen we find that all components of $\tilde{\tilde{\sigma}}$ are 0(1) or smaller, except σ_{--}, which is $0(1/\delta)$. We conclude that if $\tilde{n} \sim 0(1)$, then any solution of the system equation (13) must have $E_-^0 \sim 0(\delta)$. This, of course, breaks down if the refractive index becomes sufficiently large that $n^2 = 0(1/\delta)$. Because a large refractive index is usually associated with strong absorption, in which case a geometrical optics expansion is invalid, we restrict consideration to cases in which $n^2 \ll 1/\delta$, and then E_-^0 is indeed $0(\delta)$. It is clear that the system of equations (13) contains terms which, although determined by the zeroth-order equations, have magnitude $kv_e/\omega \sim 0(\delta)$. These are dropped from the zeroth-order equations and included as inhomogeneous terms in the first-order system. The field components E_+^0 and $E_\parallel^0$ are determined by solving (13a) and (13c) accurate to 0(1), and E_-^0 is obtained from (13b) and is $0(\delta)$.

The dispersion relation, which is obtained as the solvability condition for the homogeneous system equations (13a) and (13c), is of the form

$$D(\tilde{n}, \omega) = n_\perp^2 n^2 - 2\left(1 - \frac{\omega_{pe}^2}{\Omega_e^2}\right)n^2 + n_\perp^2 + \left(1 - \frac{\omega_{pe}^2}{\Omega_e^2}\right)\left(2 - \frac{\omega_{pe}^2}{\Omega_e^2}\right) = 0. \tag{14}$$

This is precisely the cold plasma dispersion relation evaluated at $\omega = \Omega_e$. The equations for the ray path follow directly from the dispersion relation as in (8). We have, therefore,

given a rigorous demonstration that in circumstances where waves are weakly damped, a geometrical optics description is possible near cyclotron resonance even though the Hermitian part of the dispersion tensor is large. We also see that the ray paths are given by the cold plasma dispersion relation.

However, the energy flux relation, or Poynting's theorem, is somewhat modified from the usual form shown in (9). In the first place, we have shown in reference [7] that the contribution of the particle thermal motion to the power flux (i.e., Poynting vector $\tilde{S}$) is higher order in δ. The correct form for the Poynting vector, therefore, is

$$\tilde{S} = \mathrm{Re}\left\{\frac{c}{4\pi}\hat{\tilde{E}}^{0*} \times \tilde{B}^{0}\right\} = \mathrm{Re}\left\{\frac{c}{4\pi}\hat{\tilde{E}}^{0*} \times (\tilde{n} \times \hat{\tilde{E}}^{0})\right\}$$

where $\hat{\tilde{E}}^{0}$ is the zeroth-order electric field minus the contribution from E_{-}^{0}. $[\hat{\tilde{E}}_0 = (E_+/2, -iE_+/2, E_\parallel)]$. Including all terms dropped from zero order we find a Poynting's theorem for steady-state energy flux of the form

$$\tilde{\nabla} \cdot \tilde{S} + \mathrm{Re}\,\{\hat{\tilde{E}}^{0*} \cdot \hat{\tilde{J}}^{0} + \tilde{J}^{0*} \cdot \tilde{E}_{-}^{0}\} = 0 \tag{15}$$

where $\tilde{E}_{-}^{0} = (E_-/2, iE_-/2, 0)$ and $\hat{\tilde{J}}^{0}$ is the first-order current previously dropped from the zeroth-order equations

$$\hat{J}_{+}^{0} = 0 \qquad \hat{J}_{-}^{0} = \sigma_{-+}^{1} E_{+}^{0} \qquad \hat{J}_{\parallel}^{0} = \sigma_{\parallel -}^{0} E_{-}^{0} + \sigma_{\parallel\parallel}^{1} E_{\parallel}^{0}. \tag{16}$$

$\tilde{J}^{0}$ is the zeroth-order current and σ_{-+}^{1}, $\sigma_{\parallel\parallel}^{1}$ are the terms in σ_{-+}, $\sigma_{\parallel\parallel}$, respectively, which are $0(\delta)$ in magnitude. Note that right circularly polarized component E_{-}^{0} does appear in the energy flux equation and indeed is the dominant term in absorption. Finite temperature effects must be included in calculating E_- (13b) since E_- is identically zero at resonance in cold plasma theory. The reader is referred to reference [7] for detailed derivation and for applications to cyclotron harmonic resonances as well as ion cyclotron resonances.

III. The Rays Code

We now describe the structure and operation of the computer code RAYS, which does ray tracing of electromagnetic waves in an arbitrary magnetized plasma configuration [9]. RAYS is being developed as a major part of the theoretical study of microwave heating of the ELMO Bumpy Torus (EBT) device at ORNL. As a result, the applications to date have emphasized magnetic mirror geometries and the graphics capabilities have been tailored for this application. However, other geometries have been used (slab geometry, tandem mirror, and idealizations of tokamak geometry), and we feel that the code could be readily adapted to a wide variety of plasma configurations.

The RAYS code integrates the Hamiltonian form of the geometrical optics equations for position $\tilde{x}$ and wave vector $\tilde{k}$ from initial conditions $\tilde{x}_0$ and $\tilde{k}_0$ with arc length along the ray s as the independent variable. In addition, the local electric field polarization is evaluated and quantities such as the wave damping rate or the phase path length can be integrated along the ray. The code is written in modular form, with the subroutines specifying the plasma equilibrium magnetic field and density, and subroutines specifying wave dispersion relation being independent. In this way, various models for the plasma

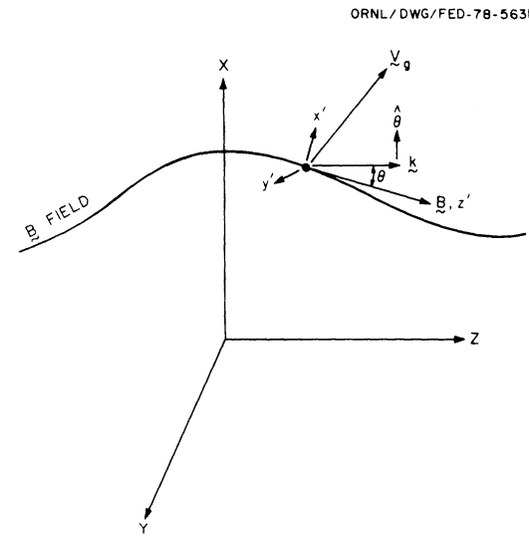

Fig. 1. Local magnetic field coordinate system used in ray tracing.

geometry and for the wave characteristics can be easily interchanged without disturbing the bulk of the program.

For time-invariant media ($\partial/\partial t = 0$), the arc length along the ray s is a convenient parameter and the ray equations (11) can be reduced to

$$\frac{d\tilde{x}}{ds} = \frac{1}{|\tilde{v}_g|}\frac{d\tilde{x}}{dt} = -\,\mathrm{sgn}\left(\frac{\partial D}{\partial \omega}\right)\frac{\partial D/\partial \tilde{k}}{|\partial D/\partial \tilde{k}|}$$

$$\frac{d\tilde{k}}{ds} = \frac{1}{|\tilde{v}_g|}\frac{d\tilde{k}}{dt} = \mathrm{sgn}\left(\frac{\partial D}{\partial \omega}\right)\frac{\partial D/\partial \tilde{x}}{|\partial D/\partial \tilde{k}|}. \tag{17}$$

In most instances RAYS integrates the ray equations using s as a parameter (17), although occasionally it proves convenient to use t (8)—for example, when all components of the group velocity vanish at a cutoff and the ray path has a nondifferentiable cusp. The group velocity is most conveniently calculated in a local coordinate system with $\hat{z}$ taken along the local magnetic field and $\hat{x}$ taken in the $\tilde{B}, \tilde{k}$ plane (Fig. 1).

The right-hand sides of the ray equations can be obtained by a straightforward but tedious differentiation of the dispersion relation. If the local dispersion relation is written in the form

$$D(\tilde{k}, \tilde{x}) = D\left[\tilde{k}, \frac{\omega_{pe}^2(\tilde{x})}{\omega^2}, \frac{\Omega_e(\tilde{x})}{\omega}, \omega\right] = 0 \tag{18}$$

where ω_{pe}^2 is the local plasma frequency, then the details of variations of the plasma equilibrium can be separated from the plasma dispersion properties. In particular, we can write

$$\frac{\partial D}{\partial \tilde{x}} = \frac{\partial D}{\partial \omega_{pe}^2}\tilde{\nabla}(\omega_{pe}^2) + \frac{\partial D}{\partial \Omega_e}\tilde{\nabla}(\Omega_e). \tag{19}$$

In order to integrate the ray equations, it is necessary to calculate the following quantities related to the spatial variation of the plasma equilibrium: $n(\tilde{x})$, $\tilde{B}(\tilde{x})$, $\tilde{\nabla} n(\tilde{x})$, and $\tilde{\nabla}\tilde{B}(\tilde{x})$. In the RAYS code this information is provided by an independent equilibrium module. It is also necessary to calculate the following quantities related to plasma dispersion: $\partial D/\partial \tilde{k}$, $\partial D/\partial \omega$, $\partial D/\partial \omega_{pe}^2$, and $\partial D/\partial \Omega_e$. In the RAYS code this information is provided by an independent dispersion module.

The coupled set of ordinary differential equations (17) are integrated in Cartesian coordinates (x, y, z, k_x, k_y, k_z) from an initial value $(x_0, y_0, z_0, k_{x0}, k_{y0}, k_{z0})$. The origin and orientation of the coordinate system are defined by the equilibrium subroutine. The initial value of the wave vector $\tilde{k}_0$ must, of course, be a solution of the local dispersion relation at the point $\tilde{x}_0$.

The dispersion relation may have multiple branches corresponding to different modes of propagation. For example, the cold plasma dispersion relation has ordinary mode and extraordinary mode branches. If $\tilde{k}_0$ is properly initialized to be a solution of the local dispersion relation, then $\tilde{k}(s)$ will remain on this branch unless a point is reached where two roots of the local dispersion relation coincide. At such a point the geometrical optics approximation breaks down and coupling can occur between the two modes. In this situation the ray tracing code follows the particular root which maintains continuity of the equations away from the coupling point; thus, one observes either zero or total mode conversion at a coupling point. Examples of mode conversion observed with the RAYS code are shown in Section IV.

Most calculations in the microwave heating study for EBT have used the Appleton-Hartree dispersion relation [6], [10], a high-frequency limit ($\omega >> \Omega_i$) of the cold plasma dispersion relation

$$D(k,\theta,\omega,\tilde{x}) = 1 - \frac{c^2k^2}{\omega^2} - \frac{2\alpha(1-\alpha)}{2(1-\alpha) - \beta\cdot\sin^2\theta \pm \Gamma(\theta,\tilde{x})} \tag{20}$$

where

$$k^2 = \tilde{k}\cdot\tilde{k},\quad \cos\theta = \tilde{k}\cdot\tilde{B}/|\tilde{k}||\tilde{B}|,$$

$$\Gamma(\omega,\theta,\tilde{x}) = [\beta^2\sin^4\theta + 4\beta(1-\alpha)^2\cos^2\theta]^{1/2},$$

$$\alpha(\omega,\tilde{x}) = \omega_{pe}^2(\tilde{x})/\omega^2,\quad \beta(\omega,\tilde{x}) = \Omega_e^2(\tilde{x})/\omega^2.$$

The +(-) sign in (20) corresponds to the ordinary (extraordinary) mode of propagation.

With this form for the dispersion relation, it is convenient to resolve the group velocity into components along $\hat{k} = \tilde{k}/|k|$ and $\hat{\theta}$:

$$\tilde{v}_g = -\frac{\frac{\partial D}{\partial k}\hat{k} + \frac{1}{k}\frac{\partial D}{\partial\theta}\hat{\theta}}{\frac{\partial D}{\partial\omega}} \tag{21}$$

where $\hat{\theta} = \tilde{k}\times(\tilde{k}\times\tilde{B})/|\tilde{k}\times(\tilde{k}\times\tilde{B})|$. The ray equations take the form

$$\frac{d\tilde{r}}{ds} = -\operatorname{sgn}\left(\frac{\partial D}{\partial\omega}\right)\frac{\frac{\partial D}{\partial k}\hat{k} + \frac{1}{k}\frac{\partial D}{\partial\theta}\hat{\theta}}{\left[\left(\frac{\partial D}{\partial k}\right)^2 + \frac{1}{k^2}\left(\frac{\partial D}{\partial\theta}\right)^2\right]^{1/2}}$$

$$\frac{d\tilde{k}}{ds} = \operatorname{sgn}\left(\frac{\partial D}{\partial\omega}\right)\frac{\frac{\partial D}{\partial\alpha}\tilde{\nabla}\alpha + \frac{\partial D}{\partial\beta}\tilde{\nabla}\beta + \frac{\partial D}{\partial\theta}\tilde{\nabla}\theta}{\left[\left(\frac{\partial D}{\partial k}\right)^2 + \frac{1}{k^2}\left(\frac{\partial D}{\partial\theta}\right)^2\right]^{1/2}}. \tag{22}$$

The right-hand sides of (22) are obtained by repeated application of the chain rule to (20). The $\tilde{\nabla}\theta$ term in the equation for $\tilde{k}(s)$ results from rotation of the local coordinate system in geometries having curved magnetic field lines. In plasmas with straight field lines, such as slab geometry, this term vanishes.

If $\tilde{k}$ becomes parallel to $\tilde{B}$, then the vector $\hat{\theta}$ which appears in $\partial D/\partial\tilde{k}$ becomes undefined. This can give rise to numerical difficulties. An alternative form of the cold plasma dispersion relation makes use of the refractive indices $n_\parallel$, $n_\perp$ and effectively avoids the need for a local magnetic coordinate system.

In terms of $n_\parallel$, $n_\perp$, the local dispersion relation can be written

$$D(n_\parallel, n_\perp, \omega, \tilde{x}) = A(n_\perp^2,\tilde{x})\,n_\parallel^4 + B(n_\perp^2,\tilde{x})\,n_\parallel^2 + C(n_\perp^2,\tilde{x}) = 0 \tag{23}$$

where

$$\tilde{n} = \frac{c\tilde{k}}{\omega}\qquad n_\parallel = \frac{\tilde{n}\cdot\tilde{B}}{B}\qquad n_\perp^2 = n^2 - \left(\frac{\tilde{n}\cdot\tilde{B}}{B}\right)^2$$

$$A = (1-\alpha)(1-\beta)$$

$$B = -2(1-\alpha)(1-\alpha-\beta) + [(1-\alpha)(1-\beta) + 1 - \alpha - \beta]\,n_\perp^2$$

$$C = (1-\alpha-\beta)\,n_\perp^4 - [(1-\alpha)(1-\alpha-\beta) + (1-\alpha)^2 - \beta]\,n_\perp^2 + (1-\alpha)[(1-\alpha)^2 - \beta].$$

The derivatives necessary for (8) are

$$\frac{\partial D}{\partial\tilde{k}} = \frac{\partial D}{\partial n_\parallel}\frac{\partial n_\parallel}{\partial\tilde{k}} + \frac{\partial D}{\partial n_\perp^2}\frac{\partial n_\perp^2}{\partial\tilde{k}}$$

$$\frac{\partial D}{\partial\tilde{x}} = \frac{\partial D}{\partial\alpha}\frac{\partial\alpha}{\partial\tilde{x}} + \frac{\partial D}{\partial\beta}\frac{\partial\beta}{\partial\tilde{x}} + \frac{\partial D}{\partial n_\parallel}\frac{\partial n_\parallel}{\partial\tilde{x}} + \frac{\partial D}{\partial n_\perp^2}\frac{\partial n_\perp^2}{\partial\tilde{x}}$$

$$\frac{\partial D}{\partial\omega} = \frac{\partial D}{\partial\alpha}\frac{\partial\alpha}{\partial\omega} + \frac{\partial D}{\partial\beta}\frac{\partial\beta}{\partial\beta} + \frac{\partial D}{\partial n_\parallel}\frac{\partial n_\parallel}{\partial\omega} + \frac{\partial D}{\partial n_\perp^2}\frac{\partial n_\perp^2}{\partial\omega} \tag{24}$$

where

$$\frac{\partial n_\parallel}{\partial\tilde{k}} = \frac{c}{\omega}\frac{\tilde{B}}{B},\quad \frac{\partial n_\perp^2}{\partial\tilde{k}} = 2\frac{c}{\omega}\left(\tilde{n} - n_\parallel\frac{\tilde{B}}{B}\right),\quad \frac{\partial n_\perp^2}{\partial\omega} = -\frac{2}{\omega}n_\perp^2,$$

$$\frac{\partial n_\parallel}{\partial\omega} = -\frac{n_\parallel}{\omega},$$

$$\frac{\partial n_\parallel}{\partial\tilde{x}} = \tilde{n}\cdot\tilde{\nabla}\left(\frac{\tilde{B}}{B}\right),\quad \frac{\partial n_\perp^2}{\partial\tilde{x}} = -2n_\parallel\frac{\partial n_\parallel}{\partial\tilde{x}},\quad \frac{\partial\alpha}{\partial\tilde{x}} = \alpha\frac{\tilde{\nabla}n_0}{n_0},$$

$$\frac{\partial\beta}{\partial\tilde{x}} = 2\beta\frac{\tilde{\nabla}B}{B},\quad \frac{\partial\alpha}{\partial\omega} = -\frac{2}{\omega}\alpha,\quad \frac{\partial\beta}{\partial\omega} = -\frac{2}{\omega}\beta.$$

The derivatives of D with respect to $\alpha, \beta, n_\perp^2$, and $n_\parallel$ are easily obtained from (23).

The electric field polarization of a given mode is a local vector quantity which is determined by the local dispersion tensor $\tilde{\tilde{D}}(\tilde{k},\tilde{r})$ (6). In the RAYS code this equation is solved in a local magnetic coordinate system $\hat{e}_x$, $\hat{e}_y$, $\hat{e}_z$, with the $\hat{z}$ axis taken along $\tilde{B}$ and the $\hat{x}$ axis taken perpendicular to $\tilde{B}$ in the $\tilde{B}, \tilde{k}$ plane.

For a cold plasma, the dispersion equation in the magnetic coordinate system is

$$\begin{bmatrix} \epsilon_1 - n^2\cos^2\theta & -i\epsilon_2 & n^2\sin\theta\cos\theta \\ i\epsilon_2 & \epsilon_1 - n^2 & 0 \\ n^2\sin\theta\cos\theta & 0 & \epsilon_3 - n^2\sin^2\theta \end{bmatrix} \begin{bmatrix} E_x \\ E_y \\ E_z \end{bmatrix} = 0 \quad (25)$$

where $\epsilon_1 = 1 - (\alpha/1 - \beta)$, $\epsilon_2 = \sqrt{\beta}\ (\alpha/1 - \beta)$, $\epsilon_3 = 1 - \alpha$, and n is a solution of the cold plasma dispersion relation. This can be solved to give eigenvectors of the form

$$\tilde{E} = \left[1, \frac{i\epsilon_2}{n_j^2 - \epsilon_1}, \frac{n^2\sin\theta\cos\theta}{n^2\sin^2\theta - \epsilon_3}\right], \quad \theta \neq \frac{\pi}{2}$$

$$\tilde{E} = \begin{bmatrix} (0,0,1) & \text{Ordinary Mode} \\ (i\epsilon_2, -\epsilon, 0) & \text{Extraordinary Mode} \end{bmatrix}, \quad \theta = \frac{\pi}{2}. \quad (26)$$

If the dispersion tensor is more complicated, such as with finite temperature effects, it is necessary to solve (6) numerically using Gaussian elimination or other techniques.

Considerable effort has been spent validating the dispersion relation modules and ODE solver by tracing rays in simple geometries for which the ray paths can be obtained analytically (e.g., slab geometry). It is also possible to obtain analytic solutions to the geometrical optics equations for certain simple nonplane geometries. For example, we have compared results obtained from the RAYS code with analytic results for the ordinary mode in cylindrical geometry [11] and found excellent agreement.

The equilibrium modules have also been extensively tested. Once the dispersion routines have been validated, a good check of the consistency between the equilibrium quantities and their gradients can be obtained by integrating the gradients along a ray path and comparing to changes in the appropriate quantities.

IV. Ray Tracing in Plane-Stratified Plasmas

In a plane-stratified medium only the component of $\tilde{k}$ in the direction of the gradients can vary, whereas the components of $\tilde{k}$ perpendicular to the gradients are constant as a consequence of Snell's law. If the direction of stratification in a cold plasma is at an arbitrary angle with respect to the magnetic field, the component of $\tilde{n}$ in the direction of the gradient is determined by a quartic equation, the Booker quartic [10], [12]. Two special cases of plane stratification which are particularly interesting are 1) perpendicular stratification–in which all gradients are in a fixed direction perpendicular to $\tilde{B}$, say in the x direction $[n_x = n_x(x, n_y, n_z)]$ and 2) parallel stratification–in which all gradients are along the magnetic field $[n_z = n_z(z, n_x, n_y)]$. We have taken the equilibrium magnetic field to be in the z direction. In the case of parallel stratification and also in perpendicular stratification when $n_y = 0$, the dispersion relation reduces from quartic to biquartic.

We consider first perpendicular stratification. If $n_y = 0$, (23) can be rearranged to give an equation for $n_x^2(\alpha, \beta, n_z^2)$ of the form

$$D = An_x^4 + Bn_x^2 + C = 0 \quad (27)$$

where

$$A = 1 - \alpha - \beta$$

$$B = [(1 - \alpha)(1 - \beta) + (1 - \alpha - \beta)]\, n_z^2 - [(1 - \alpha)(1 - \alpha - \beta) + (1 - \alpha)^2 - \beta]$$

$$C = (1 - \alpha)[(1 - \beta)\, n_z^4 - 2(1 - \alpha - \beta)\, n_z^2 + (1 - \alpha)^2 - \beta].$$

This equation can be solved immediately to give

$$(n_x^{\pm})^2 = \frac{-B \pm \sqrt{\Delta}}{2A} \quad (28)$$

where

$$\Delta = B^2 - 4AC = \alpha^2\{\beta^2 n_z^4 + 2\beta[(1 - \alpha - \beta) + (1 - \alpha)]\, n_z^2 + \beta^2\}.$$

For exactly perpendicular propagation ($n_z \to 0$), (28) reduces to

$$(n_x^{\pm})^2 = \begin{cases} 1 - \alpha \\ 1 - \dfrac{\alpha(1 - \alpha)}{1 - \alpha - \beta} \end{cases} \quad (29)$$

where the +(−) signs are associated with the ordinary (extraordinary) modes of the Appleton-Hartree dispersion relation, respectively. For $n_z \neq 0$, association of +(−) with ordinary (or extraordinary) modes is more complicated. When $\alpha > 1$, $\beta < 1$, the ordinary mode does not propagate for any n_z and both signs are associated with the extraordinary mode, corresponding to different angles of propagation with respect to the magnetic field.

It can be seen that a resonance ($n_x^2 \to \infty$) occurs in the extraordinary mode branch at the upper hybrid frequency ($A = 1 - \alpha - \beta = 0$) for arbitrary values of n_z^2. At $A \to 0$, $B \to \alpha\beta n_z^2 + \alpha(1 - \alpha) > 0$, so the resonance occurs in $(n^-)^2$. Cutoffs $n_x \to 0$ occur at values of density such that $\alpha = 1$ and $\alpha = (1 \pm \sqrt{\beta})(1 - n_z^2)$. The cutoff at $\alpha = 1$ is associated with the ordinary mode. The cutoff at $\alpha = (1 - \sqrt{\beta})(1 - n_z^2)$ is associated with the extraordinary mode; whereas when $n_z^2 < 1$, the cutoff at $\alpha = (1 + \sqrt{\beta})(1 - n_z^2)$ is in the ordinary or extraordinary mode branch according to whether $\alpha < 1$ or $\alpha > 1$, respectively. An interesting relation can be obtained by setting $n^2 = 0$ in the Appleton-Hartree dispersion relation choosing the minus sign and solving for $\sqrt{\beta}$. We find that at $\sqrt{\beta} = 1 - \alpha$, the extraordinary mode is cut off for all angles of propagation.

Fig. 2 shows typical extraordinary mode propagation in a perpendicularly stratified plasma having $\tilde{B}(\tilde{x}) = B_0[1 + (x/L)]$, where B_0 is chosen so that cyclotron resonance ($\beta = 1$) occurs at $x = 0$ and $L = 10$ cm. In cold plasma theory, a wave propagating toward cyclotron resonance from the high field side passes without impediment through cyclotron resonance to the upper hybrid resonance. When the plasma is perpendicularly stratified, cyclotron resonance is entirely a finite temperature effect. The vectors show the direction of $\tilde{k}$ turning parallel to the x direction as the resonance is approached. Rays injected from the low field side are reflected at the right-hand cutoff $\alpha = (1 - \sqrt{\beta_c})(1 - n_z^2)$ or $\beta_c = [1 - \alpha/(1 - n_z^2)]^2$.

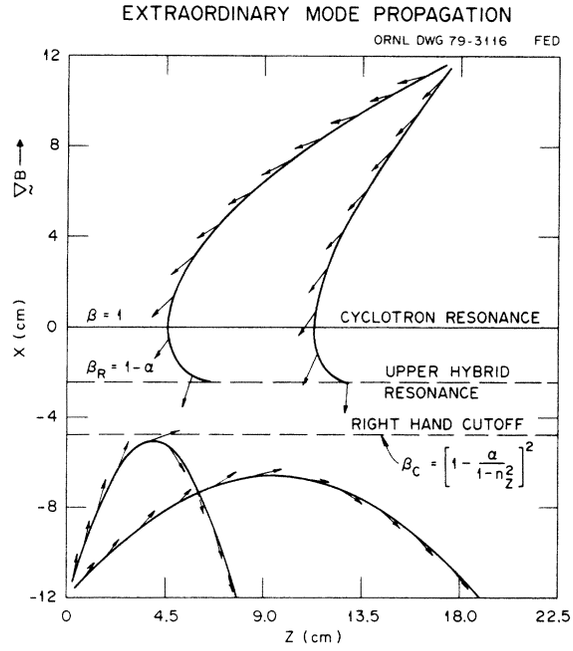

Fig. 2. Extraordinary mode rays in a perpendicular stratified plasma with linearly increasing magnetic field. Vectors indicate direction of $\tilde{k}$.

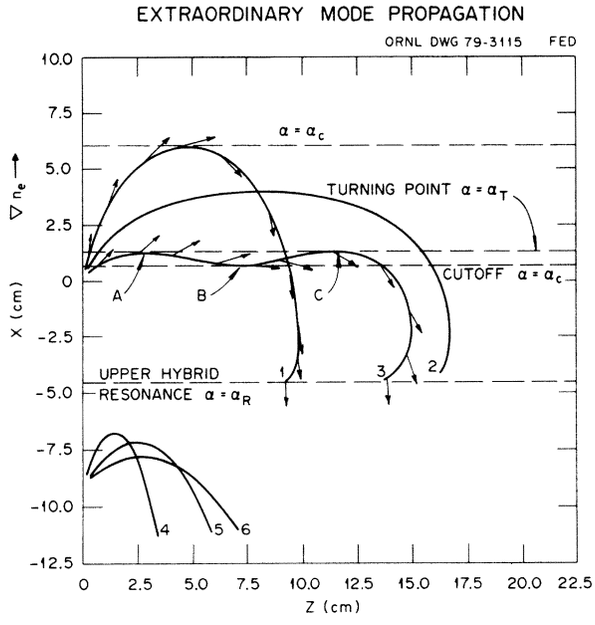

Fig. 3. Extraordinary mode rays in a perpendicularly stratified plasma with linearly increasing density.

Somewhat different behavior is observed if the magnetic field is fixed $\beta < 1$ and the density increases with x. For sufficiently large density $\alpha > \alpha_T = 1 + \beta(1 - n_z^2)^2/4n_z^2$, the discriminant Δ is negative and all solutions are evanescent. A ray propagating in the direction of increasing density reaches the point $\Delta = 0$ at which $(n_x^+)^2$ and $(n_x^-)^2$ become equal. This represents a different type of ray turning point from the usual cutoff since $C \neq 0$ and $n_x^{+2} = n_x^{-2} > 0$. Fig. 3 shows rays for this situation in a linearly increasing density $n_e(\tilde{x}) = n_0(1 + x/L)$. The quadratic form of the cold plasma dispersion relation equation (23) was used to trace these rays. The parameters were chosen such that $\sqrt{\beta} = \frac{2}{3}$, $\alpha(x = 0) = 1, L = 10$ cm.

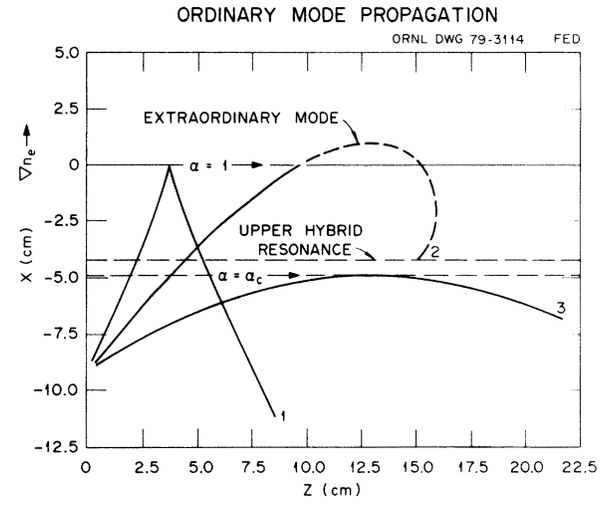

Fig. 4. Ordinary mode rays in a perpendicularly stratified plasma with linearly increasing density.

The rays were initialized to the (n_x^-) root, extraordinary mode. For rays 1 and 2, n_z^2 is small enough that the cutoff density $\alpha_c = (1 + \sqrt{\beta})(1 - n_z^2) > 1$ is less than the $\Delta = 0$ density, α_T. These rays reflect at $\alpha(x) = \alpha_c$ and continue onto the upper hybrid resonance. However, for ray 3, n_z is large, so that $\alpha(x) = \alpha_c$ is less than α_T and the cutoff is in the (n^+) branch. The ray propagates to α_T (point A); continues on the (n_x^+) branch toward decreasing x; propagates to $\alpha(x) = \alpha_c$ (point B); reflects $(n_x \to 0)$; propagates back to $\alpha(x) = \alpha_T$ (point C); continues on the (n_x^-) branch toward decreasing x; and finally approaches the upper hybrid resonance. Rays injected from the low density side are simply reflected from the right-hand cutoff $\alpha = (1 - \sqrt{\beta})(1 - n_z^2)$.

The ordinary mode also exhibits interesting and somewhat complicated behavior in perpendicular-stratified plasma. Fig. 4 shows rays initialized to the ordinary mode $(n_x = n_x^+)$ in a linearly increasing density profile. The plasma parameters were the same as for Fig. 3. When n_z is large enough that $(1 + \sqrt{\beta})(1 - n_z^2) < 1$, the cutoff occurs for $\alpha < 1$. Ray number 1 shows the reflection with continuously turning tangent. For smaller n_z we have $(1 + \sqrt{\beta})(1 - n_z^2) > 1$, so the ordinary mode cutoff occurs at $\alpha = 1$, ray number 3. In this case, however, the ray path is not smooth but has a cusp at the reflection point. The different behavior of rays 1 and 3 can be understood easily from a Poeverlein construction [10] or directly from the dispersion relation equation (27). If we factor the dispersion function D

$$D(\tilde{n}, \tilde{x}) = \{n_x^2 - n_x^+[n_z^2, \alpha(\tilde{x}), \beta(\tilde{x})]^2\} \cdot \{n_x^2 - n_x^-[n_z^2, \alpha(\tilde{x}), \beta(\tilde{x})]^2\} \tag{30}$$

we can write

$$V_{gx}(+\text{mode}) = -\frac{\omega}{c}\frac{\partial D/\partial n_x}{\partial D/\partial \omega} = -\frac{\omega}{c}\left(\frac{\partial D}{\partial \omega}\right)^{-1} 2n_x[n_x^2 - (n_x^-)^2]\Big|_{n_x = n_x^+} = -\frac{\omega}{c}\left(\frac{\partial D}{\partial \omega}\right)^{-1} 2n_x^+ \frac{\sqrt{\Delta}}{A}. \tag{31}$$

Similarly

$$V_{gz}(+\text{mode}) = \frac{\omega}{c}\left(\frac{\partial D}{\partial \omega}\right)^{-1} \frac{\partial (n_x^+)^2}{\partial n_z} \frac{\sqrt{\Delta}}{A}. \tag{32}$$

Near the reflection point $C \to 0$ we can expand $\sqrt{\Delta}$ and write $(n_x^+)^2$ as $(n_x^+)^2 \cong -(C/B)$. When the cutoff is below $\alpha = 1$, V_{gz} remains positive because near cutoff

$$\frac{\partial (n_x^+)^2}{\partial n_z} \cong -\frac{1}{B}\frac{\partial C}{\partial n_z} = -B^{-1} 4(1-\alpha) \cdot n_z[(1-\beta)n_z^2 - (1-\alpha-\beta)] > 0. \tag{33}$$

However, when the reflection occurs at $\alpha = 1$, V_{gz} is proportional to $(1-\alpha)$, which vanishes and

$$V_{gx}/V_{gz} \to \sqrt{1-\alpha}\,/\,(1-\alpha) \to \infty$$

producing the observed cusp.

Another interesting aspect of wave propagation in plasmas with perpendicular density gradient is that for a certain critical value of n_z, $n_{z\,\text{Crit}}^2 = \sqrt{\beta}/(1+\sqrt{\beta})$, the $\alpha = (1+\sqrt{\beta})\cdot(1-n_z^2)$ cutoff coincides with $\alpha = 1$. In this case the ordinary mode ($\alpha < 1$) can couple to the n_x^+ branch of the extraordinary mode ($\alpha > 1$) at the $\alpha = 1$ layer [13]-[15]. Although the geometrical optics approximation breaks down and a full wave treatment is necessary to give an accurate description of the mode conversion process, the effect can be demonstrated using geometrical optics. Ray number 2 of Fig. 4 was launched on the ordinary mode (n_x^+) branch with $n_z^2 = 0.4$ which is $n_{z\,\text{Crit}}^2$ for the parameter $\sqrt{\beta} = \frac{2}{3}$. Treating the ray equations as a coupled nonlinear system

$$\frac{dx}{dt} = -\frac{\partial D/\partial k_x}{\partial D/\partial \omega} \qquad \frac{dk_x}{dt} = \frac{\partial D/\partial x}{\partial D/\partial \omega} \tag{34}$$

we find an equilibrium point ($dx/dt = dk_x/dt = 0$) at $x = k_x = 0$. A phase-plane analysis of the system equation (34) shows that $x = k_x = 0$ is a saddle point through which a ray trajectory cannot pass. However, by adding a small perturbation to the initial value of n_x [$n_x(x = x_0) = n_x^+(x = x_0) + \delta n_x$; i.e., n_x does not satisfy $D(n_x) = 0$ exactly], one moves to a phase path of (34) which avoids $x = k_x = 0$ by a small amount. Then, depending on the sign of δn_x, the ray either reflects at $\alpha = 1$ or passes on to $\alpha > 1$ on the n_x^+ branch of the extraordinary mode. Ray 2 of Fig. 4 shows such a ray path, converting to extraordinary mode at $\alpha = 1$, proceeding to the $\Delta = 0$ turning point $\alpha = \alpha_T$, and propagating to the upper hybrid resonance on the n_x^- branch.

We turn now to wave propagation in parallel-stratified plasma. The dispersion relation for n_z^2 (23) can be solved to give

$$(n_z^\pm)^2 = \frac{-B \pm \sqrt{\Delta}}{2A} \tag{35}$$

where A, B, C are defined below (23) and $\Delta = B^2 - 4AC = \alpha^2\beta\{[2(1-\alpha) - n_x^2]^2 - (1-\beta)n_x^4\}$. For exactly parallel propagation ($n_x \to 0$), (35) reduces to

$$(n_z^\pm)^2 = 1 - \frac{\alpha}{1 \mp \sqrt{\beta}} \tag{36}$$

where the upper sign corresponds to the extraordinary mode propagation and the lower sign is ordinary mode.

Resonances ($A = 0$) occur at $\alpha = 1$ and at $\beta = 1$. To obtain the $\alpha = 1$ resonance, a gradient in density along the magnetic field is necessary. Near $\alpha = 1$ the resonant root is n^{+2}, $(n_z^+)^2 \cong \beta n_x^2/(1-\alpha)(1-\beta)$. In order that the resonance be accessible, $(n_z^+)^2 > 0$, from the low density side, $\alpha < 1$, we must have $\beta < 1$, in which case $\omega_{pe}^2/\Omega_e^2 > 1$ at resonance. The $\beta = 1$ resonance is the usual extraordinary mode cyclotron resonance which occurs at $\omega = \Omega_e$ for arbitrary n_x in parallel-stratified plasma. As β approaches 1, $B \to 2\alpha(1-\alpha) - \alpha n_x^2$. When $\alpha < 1$ and $n_x^2 < 2(1-\alpha)$, we have $B > 0$ so that the resonance is in the $(n_z^+)^2$ branch and the wave propagates [$(n_z^+)^2 > 0$] on the high field side of the resonance. On the other hand, if $n_x^2 > 2(1-\alpha)$, then $B < 0$ so that the resonance is in the n_z^{-2} branch and the wave propagates on the low field side of the resonance. An important feature of extraordinary mode propagation in parallel-stratified plasmas is that as the ray approaches the resonance from the high field side, the wave vector $\tilde{k}$ turns parallel to $\tilde{B}$ and increases rapidly in magnitude. Thus the parallel phase velocity c/n_z becomes slow, and the large number of resonant particles produces very strong cyclotron damping even for relatively low-density low-temperature plasmas. Ray tracing studies in EBT magnetic geometry, which are not parallel stratified but do have strong gradients in $|\tilde{B}|$ along the field lines, confirm that the energy in a ray is completely absorbed when the density is sufficiently high that $\omega_{pe}^2/\Omega_e^2 \cdot (c/v_e) \gtrsim 1$ [2].

Cutoffs $C \to 0$ occur for

$$n_x^2 = \begin{cases} 1-\alpha \\ \dfrac{(1-\alpha)^2 - \beta}{1-\alpha-\beta} \end{cases}. \tag{37}$$

The first cutoff $1 - \alpha - n_x^2 = 0$ is associated with the ordinary mode, whereas the second $(1-\alpha)^2 - \beta = (1-\alpha-\beta)n_x^2$ is in the extraordinary mode. Solving for β gives the field strength for the extraordinary mode cutoff $\beta_c = (1-\alpha)[1 - (\alpha/1 - n_x^2)]$ which is less than unity for $n_x^2 < 1$.

Fig. 5 shows extraordinary mode rays traced in a parallel-stratified plasma with linearly increasing magnetic field $\tilde{B}(\tilde{x}) = B_0(z/L)\hat{z}$ where B_0 is chosen so that the cyclotron resonance occurs at $z = L$. The plasma parameters were $\omega_{pe}/\omega = 0.85$ and $L = 20$ cm. The rays in Fig. 5 were calculated using the Appleton-Hartree dispersion relation module. Rays launched from the low field side (rays 1 and 2) are simply reflected at β_c depending on the value of n_x^2. Ray number 3, launched from the high field side with $n_x^2 < 2(1-\alpha)$, approaches $\Omega_e(z) = \omega$ with $\tilde{n}$ parallel to $\tilde{B}$ (i.e., $n_z \to \infty$) and $\tilde{v}_g$ perpendicular. On the other hand, ray 4, launched with $n_x^2 > 2(1-\alpha)$, penetrates through the cyclotron resonance and reaches the turning point β_T at which the discriminant vanishes, $\beta_T = 1 - [2(1-\alpha) - n_x^2]^2/n_x^4$. Here the ray moves to the $(n_z^+)^2$ branch of (35) and continues back to higher magnetic field and cyclotron resonance.

A number of other interesting phenomena can be observed in cold plane-stratified plasma if the models are complicated slightly. For example, if a constant magnetic field is chosen

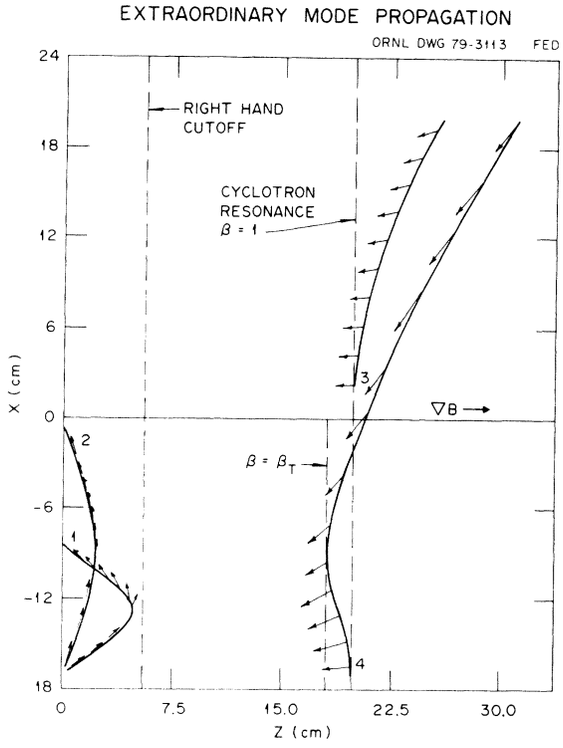

Fig. 5. Extraordinary mode rays in a parallel-stratified plasma with linearly increasing magnetic field.

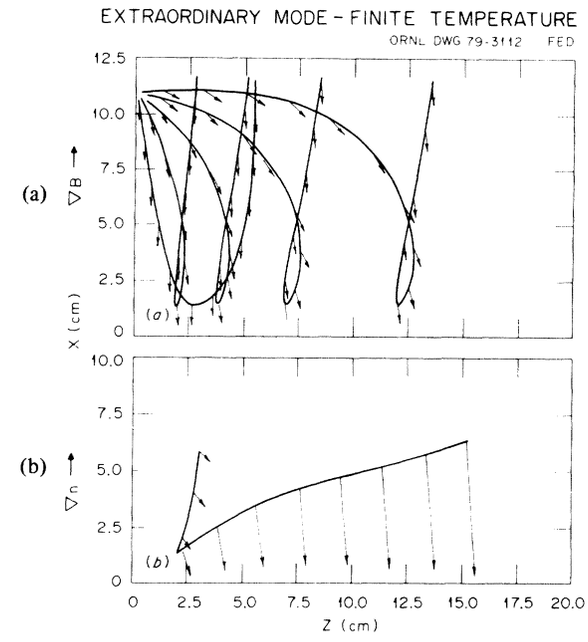

Fig. 6. Extraordinary mode propagation in a finite temperature plasma. The upper hybrid layer is at $x = 0$. (a) Linearly increasing density. (b) Linearly increasing magnetic field.

at an oblique angle to a plane density gradient, one obtains the "Spitze" for propagation along a magnetic meridian and lateral deviation for propagation at an angle to a magnetic meridian [10].

Recently we have developed a module of subroutines to calculate the derivatives of the full finite temperature dispersion relation. This dispersion relation takes the form

$$D = \det\,[\tilde{\tilde{D}}^H] = 0, \qquad D^H = \tfrac{1}{2}\,[\tilde{\tilde{D}} + \tilde{\tilde{D}}^+] \tag{38}$$

where $\tilde{\tilde{D}}$ is the dispersion tensor for a nonrelativistic isotropic Maxwellian plasma. The plasma dispersion functions $Z(\xi_n)$ and modified Bessel functions $I_n(k_\perp^2 \rho_e^2/2)$ can be included for an arbitrary number of cyclotron harmonics, $\xi_n = (\omega - n\Omega_e)/k_\parallel v_e$. Details will not be presented because the expressions are extremely complicated and the results are preliminary.

Since only the Hermitian part of the dispersion tensor is retained, this code cannot be used near cyclotron resonance. However, the formulation is valid near plasma hybrid resonances provided that the density is large enough that the hybrid resonance is well separated from cyclotron resonance. We have primarily used the code to investigate the finite temperature effects on the ray path and conversion of the extraordinary electromagnetic mode to warm plasma electrostatic modes near the upper hybrid resonance in perpendicularly stratified plasmas [16]. Fig. 6(a) shows extraordinary mode rays injected at various angles in a warm plasma ($v_e/c = 0.05$) having density increasing linearly with x, $\alpha(x) = \alpha_0(1 + x/L)$, where $\alpha_0 = 0.736$, $L = 10$ cm, and $\beta = 0.264$. With this choice of parameters, the upper hybrid resonance occurs at $x = 0$. We see that well before the upper hybrid layer is reached, the direction of $\tilde{k}$ becomes nearly perpendicular to $\tilde{B}$ and the ray trajectory reverses direction. The ray propagates back to higher density as a backward electrostatic wave with very large k_x. Fig. 6(b) shows a similar calculation for constant density ($\alpha = 0.64$) and linearly increasing magnetic field $\beta = [0.6(1 + x/7.5\text{ cm})]^2$. In this example we have plotted the magnitude of $\tilde{k}$ as well as its direction. At points away from plasma resonances, the finite temperature code on electromagnetic branches agrees extremely well with the cold plasma code.

V. Application to (EBT)

EBT-I consists of 24 toroidally linked mirror sectors having a 2:1 mirror ratio and a peak field strength on axis at the mirror throat of 9 kG. The magnetic geometry is illustrated in Fig. 7, which shows the vacuum field lines (solid) and contours of constant $|\tilde{B}|$ in the equatorial plane for a sector of EBT. Steady-state plasma is formed and heated by an ECH microwave source providing up to 60 kW at a frequency of 18 GHz and a lower off-resonance heating source providing up to 30 kW at 10.6 GHz. The current in the mirror coils is adjusted so as to produce cyclotron resonance zones $\omega = \Omega_e(\tilde{x}) = e|\tilde{B}(x)|/m_e c$ as indicated in Fig. 7. High beta annuli consisting of relativistic electrons ($T_{e\,\text{Annulus}} \sim 200$ keV) form at the midplane of each mirror sector in the vicinity of the second harmonic resonance for the 18-GHz microwaves. In addition to the high-beta annuli, the EBT plasma contains a toroidal core component of much higher density ($n_{e\,\text{Core}} \gtrsim 10\, n_{e\,\text{Annulus}}$) and lower temperature ($T_{e\,\text{Core}} \sim 150$-$600$ eV) confined by the bumpy torus magnetic field configuration [1]. An upgrade of this device (EBT-S or EBT-Scale) will soon begin operation with up to 200 kW of microwave power at 28 GHz and peak magnetic field of 14 kG. There is now great interest in the transport and scaling properties of the toroidal core plasma component in EBT to assess its potential as a fusion reactor. An appreciation for the extreme complexity

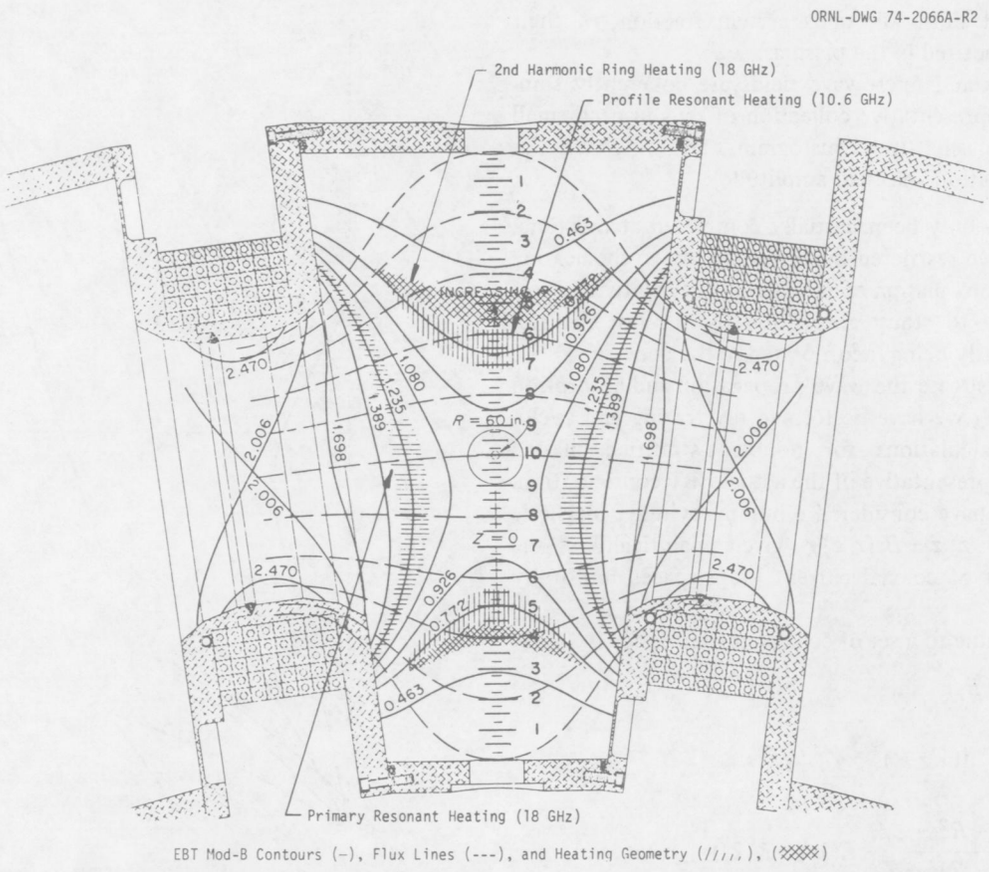

Fig. 7. Configuration of magnetic field in EBT. Two microwave frequencies (10.6 GHz and 18 GHz) are fed from the opening on the inside wall of the cavity. The not electron ring is observed to be a narrow belt encircling the local second harmonic resonance (for 18 GHz) in the midplane. The maximum microwave heating takes place at the cyclotron resonance zone (hatched area).

of the task of determining the microwave fields can be gained from Fig. 7 by observing the complicated and unsymmetrical geometry of the cavity and magnetic field lines. To solve for the fields directly as a partial differential boundary value problem is not practical for several reasons. First, the volume of the EBT vacuum vessel is so large ($v = 1.3\ m^3 \sim 10^5\ \lambda^3$) that discrete cavity modes cannot be expected to play any role and an astronomical number of mesh points would be necessary in the finite differencing scheme. Second, the plasma density is sufficiently high that plasma currents strongly affect wave propagation throughout the machine. Indeed in EBT, plasma resonances and cutoffs dominate the propagation characteristic of the microwave power. This means that in some regions the plasma dielectric constant is singular (at resonances) or complex (in evanescent regions). Third, in regions (primarily near resonances) where finite temperature effects are important, the plasma dielectric properties are not local quantities but exhibit spatial dispersion.

In view of the above difficulties, we have begun a large-scale computational effort to trace the microwave energy flow and calculate heating profiles in EBT using geometrical optics. It should be mentioned that for the current device (EBT-I), the conditions for validity of the geometrical optics approximation ($\lambda < L$) are only marginally satisfied ($\lambda \sim 1.5$–3 cm, $L \sim 3$–10 cm). However, for future devices with higher microwave frequencies and larger plasma dimensions, the geometrical optics approximation should be entirely adequate (EBT-S, $\lambda = 1.07$ cm; EBT-P, $\lambda = 0.27$ cm).

The application of geometrical optics in EBT is not without its own set of difficulties. In EBT wave resonances, cutoffs, mode conversion, and reflections from conducting walls play major roles in the propagation and absorption of microwave energy. Each of these processes is associated with the breakdown of the geometrical optics approximation. In particular, the extraordinary mode energy injected near the mirror midplane is cut off before reaching the cyclotron resonance and the ordinary mode does not significantly heat the core plasma in EBT-I. Some mechanism, therefore, must exist outside the geometrical optics model whereby extraordinary mode energy is transmitted to the high field region. The conversion of ordinary mode to extraordinary mode in the high field region upon reflection by the metal cavity appears to be the principle mechanism by which this occurs.

An outline of the basic approach being taken in making the detailed calculations is as follows.

1) The source field (at the waveguide mouth) is expanded as a superposition of plane waves or rays.
2) The rays are traced through the plasma and allowed to reflect, split (by linear mode conversion), and be absorbed.
3) Rays, or the ray trees generated by mode conversion,

are followed until all, or a certain fraction, of their energy is deposited in the plasmas.

4) The energies and microwave fields are coherently summed for a representative collection of rays in each small region of plasma (i.e., histograms are generated for energy deposition and field amplitude).

This approach has only been partially completed at this time. Up to now we have restricted our investigation to the heating of the toroidal core plasma component. The relativistic corrections necessary to study absorption by the hot electron annulus are currently being incorporated in the code.

In order to investigate the wave propagation and absorption properties of EBT, we have performed ray tracing and cyclotron damping calculations for nonplane-stratified plasma geometry more representative of the actual EBT configuration. In particular, we have considered a bumpy cylinder magnetic field, $\tilde{B}(\tilde{x}) = B_z(r, z)\,\hat{z} + B_r(r, z)\,\hat{r}$, given analytically as the field due to a set of coaxial current loops spaced uniformly along the z axis.

The exact field due to a set of coaxial current loops is

$$\bar{B}(r, z) = B_z\hat{z} + B_r\hat{r}$$

$$B_z = B_0 \sum_{j=1}^{N} [(1+R)^2 + Z_j^2]^{-1/2} \cdot \left[\frac{1 - R^2 - Z_j^2}{(1-R)^2 + Z_j^2} E(k_j) + K(k_j)\right]$$

$$B_r = -B_0 \sum_{j=1}^{N} \frac{Z_j}{R} [(1+R)^2 + Z_j^2]^{-1/2} \cdot \left[\frac{1 - R^2 + Z_j^2}{(1-R)^2 + Z_j^2} E(k_j) - K(k_j)\right] \quad (39)$$

where a = coil radius, N coils in all; $R = r/a$; $Z_j = 1/a \times$ axial distance from field point to jth coil; $k_j = \{4R/[(1+R)^2 + Z_j^2]\}^{1/2}$. E and K are complete elliptic integrals of the first and second kind. In practice the above quantities are calculated for the chosen coil geometry and then B_0 is adjusted so that on axis in the midplane ($p = z = 0$) the magnitude of $\bar{B}$ is unity. A density model for the low beta core plasma was adopted in which $n_e(\tilde{x})$ is constant along magnetic field lines and is an explicit function of the toroidal magnetic flux $\psi(r, z)$.

$$n_e(\tilde{x}) = n_0 \frac{1 - \tanh[\psi(\tilde{x}) - \psi(r_0, z=0)/\delta^2]}{1 + \tanh[\psi(r_0, z=0)/\delta^2]} \quad (40)$$

where

$$\psi(r, z) = \int_0^r dr'\, r' B_z(r', z) = \psi \sum_{j=1}^{N} \frac{R}{\sqrt{Z_j^2 + (1+R)^2}} \left[\frac{(2 - k_j^2)K(k_j) - 2E(k_j)}{k_j^2}\right].$$

Here r_0 plays the role of a plasma radius (typically $r_0 = 10$ cm, which is approximately the radius of the annulus) and δ is a gradient scale length (typically $\delta \sim 3$ cm). It should be mentioned that the magnetic field model is for vacuum fields and the density profile is essentially arbitrary. No attempt has been made to ensure that the plasma parameters correspond to self-consistent pressure equilibria. The energy deposition was calculated by integrating the imaginary part of the refractive index along a ray path

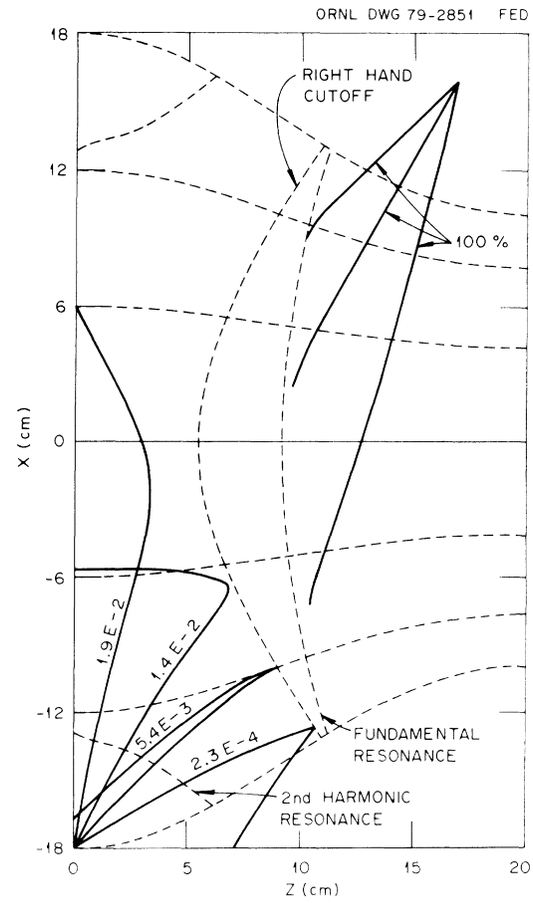

Fig. 8. Extraordinary mode propagation in EBT-I. Numbers by rays indicate fraction of power absorbed.

$$P(s) = P_0 \exp\left(-2\int_{s_0}^{s} ds'\, \tilde{k}_i \cdot \tilde{v}_g / |\tilde{v}_g|\right) \quad (41)$$

where $P(s)$ = power flux density along the ray, P_0 = initial power flux density, s = path length along the ray, $\tilde{k}_i$ = imaginary part of the wave vector, $\tilde{v}_g$ = group velocity.

The imaginary part of $\tilde{k}$ is obtained by solving the full finite temperature dispersion relation (7) numerically where both anti-Hermitian and Hermitian parts of $\tilde{\tilde{D}}$ are retained, and as many cyclotron harmonics as desired can be included.

Typical results are shown in Fig. 8, where extraordinary mode rays were injected into the bumpy cylinder equilibrium at varying angles from two points located in the equatorial plane ($y = 0$). The plasma parameters were chosen to be representative of EBT-I: $\omega/2\pi = 18$ GHz, $(\omega_{pe}/\omega)_{max} = 0.4$, and $v_e/c = 0.034$. Also shown in Fig. 8 are the magnetic field lines and equatorial cross sections of the first and second harmonic resonant surfaces and the right-hand cutoff. The fraction of power absorbed in passing through resonance is

indicated by each ray. A group of rays was injected from the low field region at the mirror midplane ($z = 0$) and outside the core plasma $x = -18$ cm. It can be seen that these rays do not penetrate to the cyclotron resonant surface but are reflected at the right-hand cutoff. Absorption at the second harmonic resonance, which is accessible, is negligible (<2 percent for the most heavily damped ray).

It is of interest to examine the fate of an extraordinary mode ray originating near the mirror throat, which, for example, might arise from depolarization of an ordinary mode ray on reflection. Fig. 8 also shows ray paths for extraordinary mode rays injected at varying angles from a point near the mirror coil. On this side, the cyclotron resonance zone is accessible. It can be seen that the rays approach the cyclotron resonance layer with $\tilde{v}_g$ nearly perpendicular to $\tilde{B}$ and $\tilde{k}$ nearly parallel to $\tilde{B}$. This is characteristic of parallel-stratified media in the cold plasma model. The rays are terminated at the point at which 99 percent of the wave power has been absorbed. For the EBT-I parameters used in the calculation, the waves are completely damped well before reaching the resonant layer.

Similar calculations have been performed for the ordinary mode, which, provided the microwave frequency is higher than the plasma frequency, is accessible to the entire plasma. In calculations of ordinary mode rays for the same equilibrium and injection geometry as shown in Fig. 8, the rays are found to be virtually straight, with only slight curvature due to density gradients. For the EBT-I parameters used, only rays within a narrow cone have more than 1 percent of the wave energy absorbed in passing through the fundamental cyclotron resonance. Absorption of the ordinary mode at the second harmonic resonance is negligible ($f \leqslant 10^{-4}$).

VI. Summary

There are difficulties in applying the usual formulation of geometrical optics to frequencies near $\omega = \Omega_e$ because of the large anti-Hermitian part of the dispersion tensor. However, we have shown that in the many cases where cyclotron absorption is weak, a consistent eikonal expansion with real rays and real $\tilde{k}$ is possible. In these cases the ray trajectories coincide with those given by cold plasma theory, but care must be taken if Poynting's theorem is used to calculate wave damping. The ray tracing code used in our ECH studies was described. Considerable flexibility is obtained if the ray equations are integrated in Cartesian coordinates and the wave dispersion properties and plasma equilibrium geometry are specified in independent modules. We discussed the various types of ray trajectories which appear in plane-stratified plasmas in the electron cyclotron range of frequencies. Considerable complication can occur even in this simple geometry. It was shown that the behavior of the ray near resonance and, in particular, the degree of absorption depends critically on the direction of gradients in the equilibrium plasma parameters. We described how geometrical optics techniques are being applied to the study of ECH problems in EBT. We find that processes outside the purview of geometrical optics, such as depolarization upon wall reflection, play an important role. Although our code is not yet developed to the level that the microwave field intensity and heating profiles can be calculated for the complicated geometry of EBT, we are able to evaluate the relative importance of the various modes of propagation and resonances. This is a considerable aid in formulating a qualitative picture of microwave heating in bumpy torus devices.

Acknowledgment

The authors would like to express appreciation for the valuable ideas and information gained in discussions with R. A. Dandl, N. H. Lazar, H. O. Eason, and C. L. Hedrick, and would also like to thank A. Kritz who was involved in formulating the finite temperature dispersion tensor module.

References

[1] A. G. Litvak, G. V. Permitin, E. V. Suvorov, and A. A. Frajmin, *Nucl. Fusion*, vol. 17, p. 659, 1977; E. Ott, B. Hui, and K. R. Chu, "Theory of cyclotron resonance heating of tokamak plasmas," NRL Rep. 4028, 1979, submitted to *Phys. Fluids.*

[2] D. B. Batchelor and R. C. Goldfinger, "A theoretical study of electron-cyclotron heating in ELMO bumpy torus," Oak Ridge Nat. Lab. Rep. ORNL/TM-6992, 1979, *Nucl. Fusion*, in press.

[3] R. A. Dandl, H. O. Eason, G. E. Guest, C. L. Hedrick, H. Ikegami, and D. B. Nelson, in *Plasma Physics and Controlled Nuclear Fusion Research (Proc. 5th Int. Conf. Tokyo, 1974)*, vol. 2. Vienna, Austria: IAEA, 1975, p. 141;
R. A. Dandl, R. A. Dory, H. O. Eason, and G. E. Guest, "Research program for plasma confinement and heating in ELMO bumpy torus devices," Oak Ridge Nat. Lab. Rep. ORNL/TM-4941, 1975;
F. W. Baity, M. C. Becker, K. H. Carpenter, J. A. Cobble, H. O. Eason *et al.*, "Summary of EBT-I experimental results," Oak Ridge Nat. Lab. Rep. ORNL/TM-6703, 1979;
R. A. Dandl, H. O. Eason, and H. Ikegami, "Electron-cyclotron heating of toroidal plasma with emphasis on results from the ELMO bumpy torus (EBT)," Oak Ridge Nat. Lab. Rep. ORNL/TM-6457, 1978.

[4] L. D. Landau and E. M. Lifshitz, in *The Classical Theory of Fields*, 3rd ed. Oxford, England: Pergamon, 1971, ch. 7.

[5] I. B. Bernstein, *Phys. Fluids*, vol. 18, p. 320, 1975.

[6] T. H. Stix, *The Theory of Plasma Waves*. New York: McGraw-Hill, 1971.

[7] H. Weitzner and D. B. Batchelor, "An eikonal expansion of the Vlasov-Maxwell equations valid near cyclotron resonance," Oak Ridge Nat. Lab. Rep. ORNL/TM-7075, *Phys. Fluids*, in press.

[8] A. I. Akhiezer, I. A. Akhiezer, R. V. Polovin, A. G. Sitenko, K. N. Stepanov *et al.*, *Plasma Electrodynamics*, vol. 1. Oxford, England: 1975.

[9] D. B. Batchelor and R. C. Goldfinger, "RAYS: A geometrical optics code for EBT," Oak Ridge Nat. Lab. Rep. ORNL/TM-6844, 1980.

[10] K. G. Budden, *Radio Waves in the Ionosphere*. Cambridge, England: Cambridge, 1961.

[11] G. A. Kriegsman, *J. Math. Phys.*, vol. 17, p. 112, 1976.

[12] K. G. Budden, *Lectures on Magnetoionic Theory*. New York: Gordon and Breach, 1964.

[13] J. Preinhalter and V. Kopecký, *J. Plasma Phys.*, vol. 10, p. 1, 1973.

[14] T. Maekawa, S. Tanaka, Y. Terumichi, and Y. Hamada, *Phys. Rev. Lett.*, vol. 40, p. 1379, 1978.

[15] H. Weitzner and D. B. Batchelor, *Phys. Fluids*, vol. 22, p. 1355, 1979.

[16] V. E. Golant and A. D. Philiya, *Sov. Phys.-Usp.*, vol. 14, p. 413, 1972 and references cited therein.